Shaoping Bai
Department of Mechanical and Manufacturing Engineering,
Aalborg University,
Denmark, Aalborg 9220
e-mail: shb@m-tech.aau.dk

Jorge Angeles
Department of Mechanical Engineering,
McGill University,
Montreal, QC, H3A 2K6, Canada
e-mail: angeles@cim.mcgill.ca

A Robust Solution of the Spatial Burmester Problem

The spatial Burmester problem is studied in this work, focusing on the synthesis of CCCC and RCCC linkages for rigid-body guidance, where R stands for revolute, C for cylindrical pair. The synthesis equations for CC and RC dyads are formulated using dual algebra. The formulation is developed in such a way that it leads to a robust solution, based on a semigraphical approach, which produces all the real solutions to the problem of CC-dyad synthesis for five given poses. This eases the equation-solving process by filtering out the complex solutions, while allowing for the handling of the special cases of none or infinitely many solutions. The synthesis procedure is illustrated with examples for four and five given poses. [DOI: 10.1115/1.4006658]

1 Introduction

The *Burmester problem* is concerned with finding the geometric parameters of a four-bar linkage whose coupler link visits a given set of finitely separated poses. The problem is also known as linkage synthesis for either *rigid-body guidance* or *motion generation*. Solutions of the Burmester problem have significant influence on the synthesis of linkages for different applications [1–3].

As a classic subject, the Burmester problem has been extensively studied in the literature [4–6]. In the case of the planar Burmester problem, Bottema and Roth [7], Hunt [8], and McCarthy [4] solved the five-pose problem by intersecting two centerpoint curves of two four-pose problems for as many subsets of four poses out of the given five-pose set, to obtain the centerpoints. Lichtenheldt [9] proposed a method based on projective geometry. Sandor and Erdman applied complex numbers [10]; Ravani and Roth [11] and Hayes and Zsombor-Murray [12], in turn, solved the problem via the kinematic mapping. Spatial path generation was addressed by C. Huang and B. Huang [13]. An approach to obtain ordered solutions was proposed in Ref. [14]. More recently, Chen et al. [15] reported a comprehensive solution of the planar Burmester problem by means of a semigraphical approach. Moreover, the spherical Burmester problem has also been extensively studied [16–22]. It is known that a linkage can be synthesized exactly for up to five given poses in both the planar and the spherical cases.

Compared with the extensive studies on the planar and spherical Burmester problems, the problem associated with the synthesis of spatial linkages for rigid-body guidance, however, has received much less attention. Very few works are available on the synthesis of spatial four-bar linkages [23,24]. Some other relevant works can be found in Refs. [24–28]. Wampler, et al. [29] developed a *continuation* method that, when applied to the synthesis of spatial mechanisms, leads to all possible solutions, real and complex. Larochelle studied the synthesis of CC *dyads*—a dyad is nothing but a link carrying one kinematic pair at each of its extremities—with four poses [28]. Murray and McCarthy investigated the determination of central-axis congruences associated with the synthesis of spatial CC dyads [30].

This paper focuses on the problem of synthesis of spatial four-bar linkages, of the CCCC and RCCC types, for rigid-body guidance. The formulation of the synthesis equations and their robust solution are given due attention. While synthesis equations were formulated by Tsai and Roth [25] for CC, RC, and RR dyads, respectively, we reformulate these equations in such a way that they lend themselves to a semigraphical solution. This formulation is shown to lead to a system of four bivariate 12th-degree polynomial equations. Using *dialytic elimination* [29], any two of these four equations can lead to a *resolvent polynomial* of a degree that can be as high as $12^2 = 144$, i.e., extremely high. The good news is that the semigraphical approach adopted here filters out the complex solutions, thereby easing the synthesis process. Moreover, the formulation can be employed for the determination of axis-congruences. A synthesis method of RCCC linkages is developed, taking into account their asymmetric topology. It is shown in the paper that the formulation proposed here works in the special cases of either none or infinitely many solutions.

The established practice to solve the problem of interest relies on *dyad synthesis*, as proposed by Roth [31,32]. In a nutshell, the four-bar linkage is regarded as composed of two dyads. One of the kinematic pairs of each dyad couples the dyad with the fixed link, the other with the coupler link. Given that the problem of dyad synthesis allows for multiple solutions, one solution linkage is composed of one of the many possible pairs obtained from the multiplicity of solutions. We follow this practice in this paper.

Dual algebra is adopted at the level of problem formulation, addressing the geometric relationships between the design task and the possible linkages. Such an approach exploits the *Principle of Transference* to derive the synthesis equations for spatial linkages using those of their spherical counterparts.

2 Problem Formulation

A generic spatial four-bar linkage of the RCCC type is depicted in Fig. 1. As the coupler link AA^* moves, while visiting m given poses, the moving axes Z_3 and Z_4, represented by the dual vectors $\hat{\mathbf{a}}_0$ and $\hat{\mathbf{a}}_0^*$ at the reference pose, attain m *locations*. A line being defined by a point and a direction, the line is short of two dimensions to occupy a rigid-body pose. Henceforth, a *line location* will be understood as given by four independent parameters, grouped in a six-dimensional array of Plücker coordinates [33]. The location of a rigid body, known as the body *pose*, requires six independent parameters. A displacement undergone by a line is also known as an *incompletely specified displacement* [34]. The m locations of the Z_3-axis are represented by the dual vectors $\hat{\mathbf{a}}_1, \ldots, \hat{\mathbf{a}}_m$, those of the Z_4-axis by $\hat{\mathbf{a}}_1^*, \ldots, \hat{\mathbf{a}}_m^*$.

Likewise, the dual vectors of the fixed axes Z_2 and Z_1 are represented by the dual vectors $\hat{\mathbf{b}}$ and $\hat{\mathbf{b}}^*$, respectively. With the foregoing model, the spatial Burmester problem is stated as:

> Find a spatial four-bar linkage that will conduct its coupler link through a set $\mathcal{S}$ of m poses, given by the orthogonal matrices $\{\mathbf{Q}_j\}_1^m$ and points $\{R_j\}_1^m$ of the coupler link, of position vectors $\{\mathbf{r}_j\}_1^m$, defined with respect to a reference pose, given by $\mathbf{Q}_0 = \mathbf{1}$ and $\mathbf{r}_0 = \mathbf{0}$.

Contributed by the Mechanisms and Robotics Committee of ASME for publication in the Journal of Mechanisms and Robotics. Manuscript received July 21, 2011; final manuscript received April 7, 2012; published online May 21, 2012. Assoc. Editor: Andrew P. Murray.

In the above statement, **1** denotes the 3×3 identity matrix and **0** the three-dimensional zero vector.

3 Synthesis of CC and RC Dyads

The solution of the spatial Burmester problem leads to the synthesis of the *RCCC linkage*, which is the main objective of this paper. The synthesis of this linkage, in turn, is achieved here based on that of the four-bar spherical linkage, recalled in Fig. 2.

For quick reference, the synthesis of the spherical linkage is recalled below. The main issue in this synthesis problem is the locations of the fixed axes $\overline{OB}$ and $\overline{OB^*}$ as well as those of their moving counterparts $\overline{OA}$ and $\overline{OA^*}$ at the *reference pose* of the coupler link. Within the approach adopted here at the outset, one RR dyad, $\widehat{AB}$ is synthesized. As the synthesis problem associated with this dyad admits up to six solutions [4], the second dyad, $\widehat{A*B*}$, is obtained from the remaining solutions. The maximum number of solutions of this problem is thus the combination number of six objects taking two at a time, namely, 15.

Furthermore, the synthesis equations of the RR dyad of interest rely on the constancy of angle α_2 throughout the various locations adopted by line $\overline{OA}$ as the coupler link visits the m given poses, which in this case reduce to orientations. Let $\mathbf{a}_0$ denote the position (unit) vector of A_0, the position of A at the reference pose of the coupler link, $\mathbf{a}_j$ denoting the position of the same point at the jth pose of the same link. Constancy of α_2 throughout the m poses thus requires

$$\mathbf{a}_j^T\mathbf{b} = \mathbf{a}_0^T\mathbf{b} \equiv \cos\alpha_2, \quad j = 1, \ldots, m \tag{1a}$$

with $\mathbf{b}$ denoting the position vector of B, and hence

$$\|\mathbf{a}_0\|^2 = \|\mathbf{b}\|^2 = 1 \tag{1b}$$

Moreover, $\mathbf{a}_j$ is obtained as a rotation of $\mathbf{a}_0$ via the rotation matrix $\mathbf{Q}_j$

$$\mathbf{a}_j = \mathbf{Q}_j\mathbf{a}_0, \quad j = 1, \ldots, m \tag{1c}$$

With this background, we can now undertake the synthesis of the CC and RC dyads.

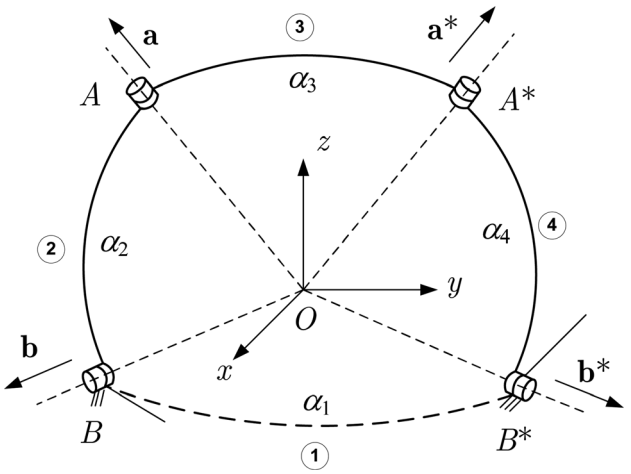

Fig. 2 The spherical 4R linkage

Some fundamental concepts of dual algebra, adopted in this work to formulate the synthesis problem, are summarized in Appendix A. For more details, the reader is directed to the pertinent literature [4,35–37].

With reference to the spatial linkage of Fig. 1, joint axes Z_3 and Z_4, which define uniquely the coupler link, undergo spatial motion while visiting the m given poses. The spatial displacement of the moving axis Z_3 in terms of dual vectors can be described by

$$\hat{\mathbf{a}}_j = \hat{\mathbf{Q}}_j\hat{\mathbf{a}}_0, \quad j = 1, \ldots, m \tag{2}$$

where $\hat{\mathbf{a}}_0$ is the dual representation of line Z_3 at the reference pose of link 3, while $\hat{\mathbf{Q}}_j$ is the *dual orthogonal matrix* representing the spatial displacement of Z_3, namely

$$\hat{\mathbf{a}}_0 = \mathbf{a}_0 + \varepsilon\bar{\mathbf{a}}_0, \quad \hat{\mathbf{Q}}_j = \mathbf{Q}_j + \varepsilon\bar{\mathbf{Q}}_j \tag{3}$$

with $\mathbf{a}_0$ denoting the unit vector parallel to Z_3 at its reference pose and $\bar{\mathbf{a}}_0$ the *moment* of the same axis with respect to the origin O_1 of the frame $\{X_1,Y_1,Z_1\}$. Moreover, $\mathbf{Q}_j$ is the proper orthogonal

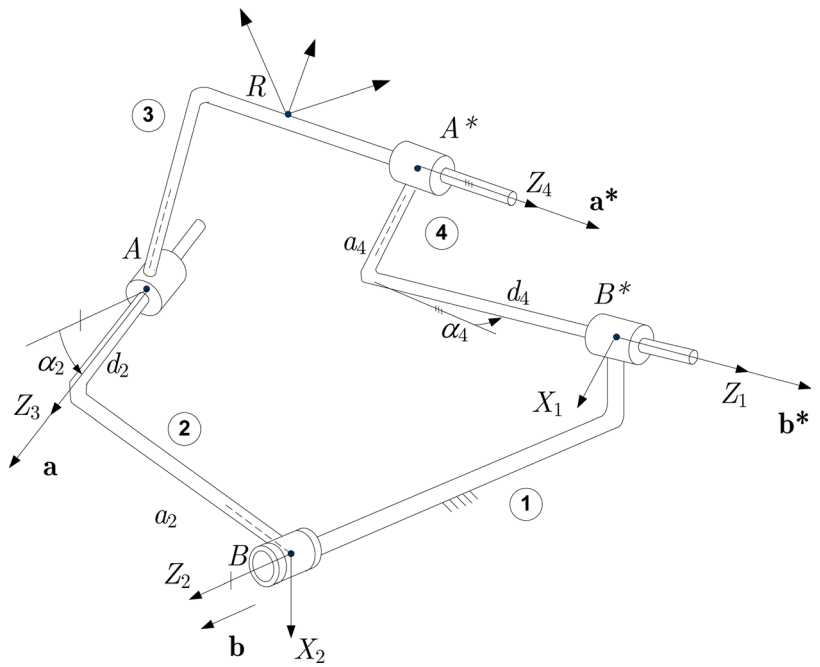

Fig. 1 The RCCC linkage

matrix that rotates the coupler link from its 0th to its jth attitude. In addition, $\bar{\mathbf{Q}}_j$ is the product of a *translation matrix* $\mathbf{R}_j$ by $\mathbf{Q}_j$, i.e.,

$$\bar{\mathbf{Q}}_j = \mathbf{R}_j \mathbf{Q}_j \tag{4}$$

with $\mathbf{R}_j$ defined as the *cross-product matrix* of vector $\mathbf{r}_j$, i.e., $\mathbf{R}_j = \mathrm{CPM}(\mathbf{r}_j) = \partial(\mathbf{r}_j \times \mathbf{v})/\partial(\mathbf{v})$, for any vector $\mathbf{v} \in \mathbb{R}^3$.

Given that the pose of Z_3 with respect to Z_2 remains constant throughout the motion of the coupler link, the dual angle between the two axes remains constant, and hence

$$\hat{\mathbf{a}}_j^T \hat{\mathbf{b}} = \cos(\alpha_2 + \varepsilon a_2) \equiv \cos\alpha_2 - \varepsilon a_2 \sin\alpha_2, \quad j = 0, \ldots, m \tag{5}$$

where

$$\hat{\mathbf{b}} = \mathbf{b} + \varepsilon \bar{\mathbf{b}} \tag{6}$$

with α_2, a_2, and $\mathbf{b}$ shown in Fig. 1, while vector $\bar{\mathbf{b}}$ denotes the moment of Z_2 with respect to O_1. Subtracting the 0th equation from the m remaining equations (5) leads to

$$(\hat{\mathbf{a}}_j - \hat{\mathbf{a}}_0)^T \hat{\mathbf{b}} = 0, \quad j = 1, \ldots, m \tag{7}$$

which, upon expansion into its primal and dual parts, for $j = 1, \ldots, m$, yields

$$\mathbf{a}_0^T(\mathbf{Q}_j^T - \mathbf{1})\mathbf{b} = 0 \tag{8a}$$

$$\mathbf{a}_0^T \bar{\mathbf{Q}}_j^T \mathbf{b} + \mathbf{a}_0^T(\mathbf{Q}_j^T - \mathbf{1})\bar{\mathbf{b}} + \bar{\mathbf{a}}_0^T(\mathbf{Q}_j^T - \mathbf{1})\mathbf{b} = 0 \tag{8b}$$

whose unknowns, $\mathbf{a}_0$, $\bar{\mathbf{a}}_0$, $\mathbf{b}$, and $\bar{\mathbf{b}}$, are subject to the constraints

$$\mathbf{a}_0^T \bar{\mathbf{a}}_0 = 0; \quad \mathbf{b}^T \bar{\mathbf{b}} = 0 \tag{9a}$$

$$\|\mathbf{a}_0\|^2 = 1; \quad \|\mathbf{b}\|^2 = 1 \tag{9b}$$

We thus have two real sets of equations, Eq. (8*a*) for the primal and Eq. (8*b*) for the dual part. Of these, Eq. (8*a*) involves only unit vectors of the joint axes, while Eq. (8*b*) involves both unit and moment vectors. Therefore, while Eq. (8*a*) is dimensionless, Eq. (8*b*) has units of length. Following Ref. [4], we call the first set the *direction*, the second the *moment equations*. Both sets stand for the basic geometric constraints on different dyads, including CC, RC, and RR. Furthermore, Eq. (8*a*) are nothing but the synthesis equations for the spherical four-bar linkage, illustrated in Fig. 2, under motion generation[1].

Equation (8*b*) can have a different, more useful form. It is convenient to introduce the position vectors of points on the axes of rotation as design variables, namely

$$\bar{\mathbf{a}}_0 = \mathbf{r}_{A0} \times \mathbf{a}_0; \quad \bar{\mathbf{b}} = \mathbf{r}_B \times \tag{10}$$

where $\mathbf{r}_{A0}$ and $\mathbf{r}_B$ are the position vectors of points A_0 and B on the two axes in the frame $\{X_1, Y_1, Z_1\}$. In light of Eq. (10), Eq. (8*b*), after some manipulations, can be rewritten as

$$(\mathbf{r}_{Aj} - \mathbf{r}_B)^T(\mathbf{a}_j \times \mathbf{b}) - (\mathbf{r}_{A0} - \mathbf{r}_B)^T(\mathbf{a}_0 \times \mathbf{b}) = 0, \quad j = 1, \ldots, m \tag{11}$$

where $\mathbf{a}_j = \mathbf{Q}_j \mathbf{a}_0$, while $\mathbf{r}_{Aj} = \mathbf{r}_j + \mathbf{Q}_j \mathbf{r}_{A0}$. The above equation describes the constancy of the projection of the line segment defined by two points on the two axes onto their common normal.

[1]That is, if abstraction is made of the translation of the rigid body when formulating the problem stated in Section 2, then points R_j, for $j = 1, \ldots, m$, coincide with point R_0, and the problem at hand becomes one of spherical synthesis.

3.1 The Synthesis of the CC Dyad. The CC dyad under synthesis consists of a rigid link that is coupled to ground via one C joint and to the coupler link via a second C joint. The dyad can be geometrically regarded as a link composed of two skew lines, joined to each other by means of a third line, their common normal, for example. A CC dyad is thus determined once the two skew lines are known. The problem of CC-dyad synthesis thus reduces to locating the two joint axes. The latter can be uniquely described by means of the dual vectors $\hat{\mathbf{a}}_0$ and $\hat{\mathbf{b}}$, which comprise a total of 12 scalar components. Note that $\mathbf{a}_0$ and $\mathbf{b}$ are unit vectors, while a line can be regarded as a zero-pitch screw [4], as expressed by Eqs. (9*a*) and (9*b*). Those four scalar constraints thus reduce the number of independent variables to only eight.

3.1.1 Five-Pose Synthesis ($m = 4$). Equations (8*a*) and (8*b*) lead to $2m$ constraint equations for m given poses. For the number of the latter to yield as many equations as unknowns, i.e., eight, one must have $2m = 8$. The system thus admits exact solutions for CC dyads in the case of $m = 4$, i.e., with five given poses.

Knowing that the direction equations are independent of the moment equations, we can find first the direction vectors through Eq. (8*a*). These equations, identical to those of the Burmester problem for spherical linkages, admit at most six real solutions. With each such solution, the moment equations become linear in the moments, namely

$$\mathbf{p}_j^T \bar{\mathbf{a}}_0 + \mathbf{q}_j^T \bar{\mathbf{b}} = w_j, \quad j = 1, \ldots, m \tag{12}$$

with

$$\mathbf{p}_j = (\mathbf{Q}_j^T - \mathbf{1})\mathbf{b}, \quad \mathbf{q}_j = (\mathbf{Q}_j - \mathbf{1})\mathbf{a}_0, \quad w_j = -\mathbf{a}_0^T \bar{\mathbf{Q}}_j^T \mathbf{b} \tag{13}$$

Equations (9*a*) and (12) amount to six linear equations for six unknowns in the case of $m = 4$, thus defining a unique pair of moments, $\bar{\mathbf{a}}_0$ and $\bar{\mathbf{b}}$, in the absence of singularities.

The six linear equations (9*a*) and (12) can be cast in vector form, namely

$$\mathbf{M}\mathbf{x} = \mathbf{w} \tag{14}$$

where

$$\mathbf{M} = \begin{bmatrix} \mathbf{p}_1^T & \mathbf{q}_1^T \\ \vdots & \vdots \\ \mathbf{p}_4^T & \mathbf{q}_4^T \\ \mathbf{a}_0^T & \mathbf{0}^T \\ \mathbf{0}^T & \mathbf{b}^T \end{bmatrix}, \quad \mathbf{x} = \begin{bmatrix} \bar{\mathbf{a}}_0 \\ \bar{\mathbf{b}} \end{bmatrix}, \quad \mathbf{w} = \begin{bmatrix} w_1 \\ \vdots \\ w_4 \\ 0 \\ 0 \end{bmatrix} \tag{15}$$

and hence, $\mathbf{M}$ is a 6×6 matrix.

So far, we have reformulated the synthesis equations for CC dyads. Apparently, the spatial linkage synthesis with CC dyads is based essentially on the Burmester problem for spherical linkages. Note that Eq. (8*a*) also represent the synthesis equations for spherical four-bar linkages, which can be readily solved with a semigraphical approach, as reported in Ref. [20].

3.1.2 Four-Pose Synthesis ($m = 3$). If only four poses are given, a total of six equations are obtained from Eqs. (8*a*) and (8*b*). In this case, the system of synthesis equations is underdetermined, and hence, infinitely many solutions are possible. These solutions can be regarded as sets of lines, called *congruences*, which define the moving and fixed axes. The generation of line congruences is described in Sec. 4.3.

3.2 The RC Dyad. An RC dyad is composed of a revolute and a cylindrical joint. The constraints for a CC spatial dyad also apply to an RC dyad. Moreover, compared with a CC dyad, an RC

dyad is subject to one more constraint: the sliding s_j along the fixed axis, shown in Fig. 3, is zero. This constraint can be expressed in terms of the dual vector of the common normal.

According to Eq. (52) of Appendix A, for the jth pose, the common normal to $\mathcal{L}_a$ and $\mathcal{L}_b$ is

$$\hat{\mathbf{n}}_j = \mathbf{n}_j + \varepsilon\bar{\mathbf{n}}_j, \quad j = 0, \ldots, m \tag{16}$$

with

$$\mathbf{n}_j = \frac{1}{\sin\alpha_{2j}}(\mathbf{a}_j \times \mathbf{b}) \tag{17}$$

$$\bar{\mathbf{n}}_j = \frac{1}{\sin\alpha_{2j}}(\mathbf{a}_j \times \bar{\mathbf{b}} + \bar{\mathbf{a}}_j \times \mathbf{b}) - \frac{a_{2j}\cos\alpha_{2j}}{\sin^2\alpha_{2j}}(\mathbf{a}_j \times \mathbf{b}) \tag{18}$$

where a_{2j} and α_{2j} are the distance and angle between $\mathcal{L}_a$ and $\mathcal{L}_b$, respectively, at the jth given pose. Now, by virtue of the link rigidity, $a_{2j} = a_{20} \equiv a_2$ and $\alpha_{2j} = \alpha_{20} \equiv \alpha_2$, the above equations then becoming

$$\mathbf{n}_j = \frac{1}{\sin\alpha_2}(\mathbf{a} \times \mathbf{b}) \tag{19}$$

$$\bar{\mathbf{n}}_j = \frac{1}{\sin\alpha_2}(\mathbf{a}_j \times \bar{\mathbf{b}} + \bar{\mathbf{a}}_j \times \mathbf{b}) - \frac{a_2\cos\alpha_2}{\sin^2\alpha_2}(\mathbf{a}_j \times \mathbf{b}) \tag{20}$$

The dual angle between two poses of the common normals, $\hat{\mathbf{n}}_j$ and $\hat{\mathbf{n}}_0$, can be found from

$$\cos\hat{\beta}_j = \hat{\mathbf{n}}_j^T\hat{\mathbf{n}}_0, \quad j = 1, \ldots, m \tag{21}$$

where $\hat{\beta}_j = \beta_j + \varepsilon s_j$ with β_j and s_j denoting the jth rotation and the jth sliding of the joint, respectively. Equating the dual parts of the expanded equation (21) leads to

$$-s_j\sin\beta_j = \frac{1}{\sin^3\alpha_2}(A_j a_2\cos\alpha_2 - B_j\sin\alpha_2) \tag{22}$$

with

$$A_j = 2\,(\mathbf{a}_0 \times \mathbf{b})^T(\mathbf{a}_j \times \mathbf{b}) \tag{23}$$

$$B_j = (\mathbf{a}_0 \times \mathbf{b})^T(\mathbf{a}_j \times \bar{\mathbf{b}} + \bar{\mathbf{a}}_j \times \mathbf{b}) + (\mathbf{a}_j \times \mathbf{b})^T(\mathbf{a}_0 \times \bar{\mathbf{b}} + \bar{\mathbf{a}}_0 \times \mathbf{b}) \tag{24}$$

For RC dyads, $s_j = 0$, while, for spatial dyads, α_2 does not vanish because their synthesis is based on that of a spherical linkage, for which no pair of revolute axes are parallel; hence, Eq. (22) yields

$$A_j a_2\cos\alpha_2 - B_j\sin\alpha_2 = 0, \quad j = 1, \ldots, m \tag{25}$$

which is the set of constraint equations needed to guarantee the vanishing of the sliding on the fixed axis.

For an RC spatial dyad, we have constraint equations (8*a*), (8*b*), and (25), which account for $3m$ equations for m poses. Note that the problem bears eight independent unknowns, which means that an RC-dyad synthesis problem admits exact solutions for $m = 8/3$. Since a fractional number of given poses does not make sense, the number of poses has to be an integer, $m = 2$, in which case the number of variables exceeds that of constraint equations by two, infinitely many solutions thus being available.

An RR dyad, consisting of two revolute joints, requires additional constraint equations to those of the RC dyad. The additional equations pertain to the vanishing of the second sliding, namely, d_j of Fig. 3. Alternatively, the constraint equations can be derived from the geometric relationship between two axes, as included in Appendix B for the interested reader. The formulation involves $4m + 2$ equations for m poses. On the other hand, there are 10 independent variables, with four direction and six position variables. For $m = 2$, i.e., three poses, an RR spatial dyad admits exact solutions, as Tsai and Roth found [25].

4 Synthesis of Four-bar Linkages

A two-degree-of-freedom (two-dof) CCCC linkage can be built with two CC dyads. As shown in Sec. 3.1, each dyad admits exact solutions for $m = 4$, i.e., for five poses. A CCCC linkage can thus be synthesized exactly for $m = 4$.

An RCCC linkage is different from a CCCC linkage, the former having one dof, the latter two. Moreover, an RCCC linkage has an asymmetrical topology. As discussed in Sec. 3, an RC dyad admits exact solutions only for three given poses. Hence, there are no exact solutions for the RCCC linkage synthesis when $m > 2$.

4.1 A Semigraphical Approach to Direction-Equation Solving. The direction equations (8*a*) can be solved by means of the semigraphical approach introduced for the synthesis of spherical four-bar linkages [20]. In this approach, *spherical coordinates* on the unit sphere, namely, *longitude* and *latitude*, are used to describe the unit vectors of all four directions. Let, then, θ_a and

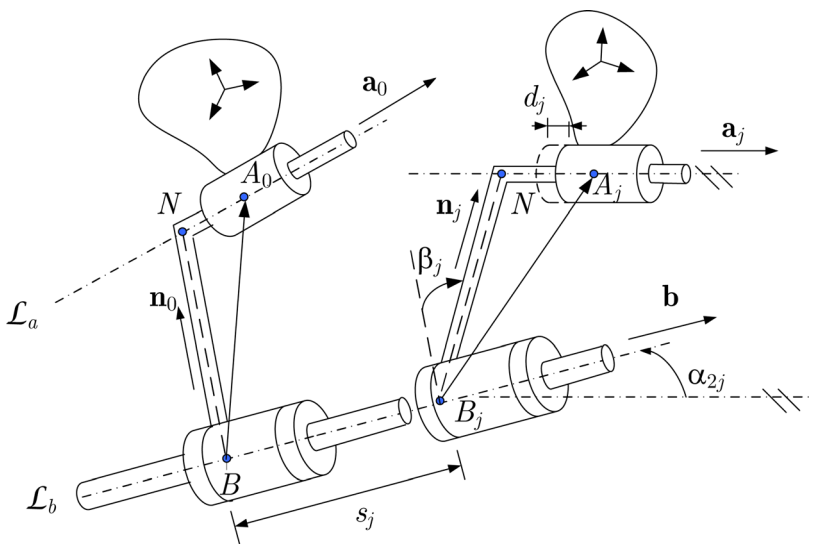

Fig. 3 A CC spatial dyad, which becomes an RC dyad if the sliding s_j vanishes

φ_a be the longitude and the latitude of a point on the unit sphere defining $\mathcal{L}_a$, θ_b and φ_b the counterpart coordinates for the point defining $\mathcal{L}_b$. Hence

$$\mathbf{a}_0 = \begin{bmatrix} \cos\phi_a \cos\theta_a \\ \cos\phi_a \sin\theta_a \\ \sin\phi_a \end{bmatrix}, \quad \mathbf{b} = \begin{bmatrix} \cos\phi_b \cos\theta_b \\ \cos\phi_b \sin\theta_b \\ \sin\phi_b \end{bmatrix} \tag{26}$$

Further, the direction equations are rewritten as

$$\mathbf{c}_j^T \mathbf{b} = 0, \quad j = 1, \ldots, 4 \tag{27}$$

or, upon assembling all four equations in array form,

$$\mathbf{C}\mathbf{b} = \mathbf{0}, \quad \mathbf{C} = \begin{bmatrix} \mathbf{c}_1^T \\ \mathbf{c}_2^T \\ \mathbf{c}_3^T \\ \mathbf{c}_4^T \end{bmatrix} \tag{28}$$

where

$$\mathbf{c}_j = (\mathbf{Q}_j - \mathbf{1})\mathbf{a}_0 \tag{29}$$

As vector $\mathbf{b}$ is of unit magnitude, it cannot vanish, and hence, $\mathbf{C}$ must be rank-deficient; therefore, its four 3×3 subdeterminants must vanish

$$\Delta_j(\mathbf{a}_0) \equiv \det(\mathbf{C}_j) = 0, \quad j = 1, \ldots, 4 \tag{30}$$

with $\mathbf{C}_j$ denoting the 3×3 matrix obtained upon deleting the jth row from $\mathbf{C}$. Now the four determinant equations (30) in $\mathbf{a}_0$ become equations in the trigonometric functions of φ_a and θ_a. They define four contours $\mathcal{C}_j$ in the $\varphi_a - \theta_a$ plane. If the four contours are plotted in the square $-\pi/2 \le \varphi_a \le \pi/2, -\pi/2 \le \theta_a \le \pi/2$, then the intersections of the four contours yield *all the real solutions* sought.[2] There can be six, four, two or no real solutions, in general [4,18]. Two special cases, zero and infinitely many solutions, are noted. In the case of zero solutions, no common intersection of the four contours appears in the superimposed plots. At the other end of the spectrum, infinitely many solutions are possible when either φ_a or φ_b is identical to $\pm\pi/2$, which thus yields points at a pole of the unit sphere; poles are known to admit any possible longitude—at the poles of the Earth, any time is good, as all time zones converge there!

The intersections are estimated by inspection on the four contours. These estimates can then be refined if used as initial guesses of an iterative procedure to find the roots of *any* pair of the four foregoing equations. As there are as many as six possible such pairs, the choice of the two equations depends on the arbitrariness of the designer. If the choice turns out to be lucky, i.e., if the two contours intersect at "sharp enough" angles, then the solution will be reliable enough; else, the solution may be either unreliable—contours intersect at almost-coincident contour segments—or impossible to find—contours are tangent to each other at the intersection point. To help the designer, a least-square approximation of the overdetermined system of four nonlinear equations in only two unknowns is recommended here: in fact, the four contours will not intersect at one common point because of roundoff error; however, nonlinear least squares will return the most likely, and hence, the most reliable estimate of the intersection. This is the same approach taken by engineers in problems of triangulation.

Once $\mathbf{a}_0$ is known, $\mathbf{c}_j$, for $j = 1, \ldots, 4$, can be computed from Eq. (29), and hence, the 4×3 matrix $\mathbf{C}$ is available. Vector $\mathbf{b}$ can then be found as the unit vector spanning the nullspace of $\mathbf{C}$, which can be determined using, e.g., the QR-decomposition[3] of $\mathbf{C}$ [38]. While this approach is sound, it entails one drawback: any roundoff error incurred in computing $\mathbf{C}$ is propagated into the computation of $\mathbf{b}$. A robust approach consists in computing $\mathbf{b}$ independent from the computation of $\mathbf{a}_0$. In this vein, the foregoing procedure is paraphrased, as applicable to the other end of the dyad, which is done by rewriting Eq. (8a) as

$$\mathbf{D}\mathbf{a}_0 = \mathbf{0}, \quad \mathbf{D} = \begin{bmatrix} \mathbf{d}_1^T \\ \mathbf{d}_2^T \\ \mathbf{d}_3^T \\ \mathbf{d}_4^T \end{bmatrix} \tag{31}$$

whence the determinant equations to find θ_b and φ_b are derived as

$$\Delta_j(\mathbf{b}) \equiv \det(\mathbf{D}_j) = 0, \quad j = 1, \ldots, 4 \tag{32}$$

with $\mathbf{D}_j$ denoting the 3×3 matrix obtained upon deleting the jth row from $\mathbf{D}$. Note that $\mathbf{d}_j = \left(\mathbf{Q}_j^T - \mathbf{1}\right)\mathbf{b}$.

4.2 Solving the Linear Equations of the Moment Variables. Once the unit vectors $\mathbf{a}_0$ and $\mathbf{b}$ are known, a system of linear equations in six unknowns can be obtained from Eq. (14) for the moments $\bar{\mathbf{a}}_0$ and $\bar{\mathbf{b}}$. Now, as Eq. (14) is a system of $m+2$ linear equations for six moment variables, a unique set of solutions for $\bar{\mathbf{a}}_0$ and $\bar{\mathbf{b}}$ can be found for $m = 4$.

4.3 Congruences of Fixed and Moving Axes. In the synthesis of planar four-bar linkages with four given poses, circlepoint- and centerpoint curves can be generated to select pivoting points for moving and fixed-joint centers, respectively. In analogy with the planar case, sets of lines for the moving and fixed axes can be determined. These sets of lines, called *congruences*, define the moving and fixed axes of the CC dyads that guide a rigid body through four given poses.

Murray and McCarthy developed a parametrization technique for the central-axis congruence for the problem of four-pose rigid-body guidance, utilizing the dual crank angle of rotation as generation parameter [30]. Larochelle developed a procedure to determine both the fixed and moving congruences [28].

We propose below an alternative method of defining and generating congruences of lines that may be used as fixed and moving axes. The method takes advantage of the three constraint equations, as outlined below.

Referring to Eq. (32) with $m = 3$, $\mathbf{C}$ becomes a 3×3 matrix, which must be singular. This means that, under the four given poses

$$F(\mathbf{a}_0) \equiv \det(\mathbf{C}) = (\mathbf{c}_1 \times \mathbf{c}_2)^T \mathbf{c}_3 = 0 \tag{33}$$

Equation (33) defines a conic surface in Cartesian space. Its intersection with the unit sphere yields a spherical curve, which is called the *spherical circlepoint curve* [4]. Each point on the curve defines a possible unit vector for the moving axis.

Likewise, the equation for the unit vector of the fixed axis has the form

$$G(\mathbf{b}) \equiv \det(\mathbf{D}) = (\mathbf{d}_1 \times \mathbf{d}_2)^T \mathbf{d}_3 = 0 \tag{34}$$

The intersection of the cubic surface described by the above equation with the unit sphere yields the *spherical centerpoint curve*. Each point on the curve corresponds to a unit vector for the fixed axis.

Note that the centerpoint and the circlepoint curves are linked through the direction constraint equation (8*a*). This means that

[2]Here, of course, the *antipodal* solutions of those lying in the square of side-length π are excluded.

[3]Every $m \times n$ matrix with $m \ge n$ can be factored into a $m \times m$ orthogonal matrix $\mathbf{Q}$ and an upper-triangular matrix $\mathbf{R}$ [38].

each point on one of the two curves has its unique matching point on the other curve.

The dual-vector parts of the two axes, i.e., the moments $\bar{\mathbf{a}}_0$ and $\bar{\mathbf{b}}$, can be found from Eq. (14). However, for $m=3$, $\mathbf{M}$ of Eq. (14) is of 5×6, and the system is underdetermined. A sixth row $\mathbf{m}_6^T$ is added to matrix $\mathbf{M}$, this row being defined as

$$\mathbf{m}_6^T = [1, 0, 0, 0,\ 0,\ 0] \tag{35}$$

and, correspondingly, the right-hand side of Eq. (14) becomes

$$\mathbf{w} = [w_1, \ldots, w_m,\ 0,\ 0, \lambda]^T \tag{36}$$

which means that the x-component $(\bar{\mathbf{a}}_0)_x$ of $\bar{\mathbf{a}}_0$ is assigned a variable value λ. If the choice of $\mathbf{m}_6$ happens to render $\mathbf{M}$ singular, then another component of $\bar{\mathbf{a}}_0$ should be chosen instead.

Because of the algebraic coupling between $\bar{\mathbf{a}}_0$ and $\bar{\mathbf{b}}$, moreover, the latter also turns out to be a function of parameter λ. Equation (14) thus yields, in this case, the moments sought as linear functions of parameter λ. We thus obtain solution axes in the form of Plücker coordinates $[\mathbf{a}_0^T\ \bar{\mathbf{a}}_0^T(\lambda)]^T$ and $[\mathbf{b}^T\ \bar{\mathbf{b}}^T(\lambda)]^T$, each standing for a set of parallel lines located on the same plane.

Once vectors $\mathbf{a}_0$, $\bar{\mathbf{a}}_0$, $\mathbf{b}$, and $\bar{\mathbf{b}}$ are available, the position vectors $\mathbf{r}_{A0}$ and $\mathbf{r}_B$, as introduced in Eq. (10), can be computed. However, the foregoing vector equations do not determine the position vectors sought uniquely, as each equation comprises only two linearly independent scalar equations. To define one particular solution, the condition is imposed that the solution sought be closest to the origin, thereby introducing one additional equation for $\mathbf{r}_{A0}$, $\mathbf{a}_0^T\mathbf{r}_{A0}=0$, and one for $\mathbf{r}_B$, $\mathbf{b}^T\mathbf{r}_B=0$. In this way, four linear equations for each position vector are derived, of which three are linearly independent, the fourth being consistent with the other three. The results are

$$\mathbf{r}_{A0} = \mathbf{a}_0 \times \bar{\mathbf{a}}_0, \quad \mathbf{r}_B = \mathbf{b} \times \bar{\mathbf{b}} \tag{37}$$

thereby completing all calculations required.

5 Examples

We include here examples, solved with Maple, of spatial linkage synthesis to demonstrate the foregoing method. The given poses are displayed in Table 1, where the orientation is described with *natural invariants* [39], i.e., the unit vector $\mathbf{e}_j$ of the axis of rotation and the angle of rotation φ_j, at the jth pose. The rotation matrix at this pose then takes the form [39]

$$\mathbf{Q}_j = \mathbf{1} + \mathrm{s}\varphi_j\mathbf{E}_j + (1-\mathrm{c}\varphi_j)\mathbf{E}_j^2 \tag{38}$$

where $\mathbf{E}_j$ denotes the cross-product matrix of $\mathbf{e}_j$, while $\mathrm{c}\varphi_j$ and $\mathrm{s}\varphi_j$ stand for cos φ_j and sin φ_j, respectively.

5.1 Five-Pose Case. For starters, the direction unit vectors of the axes are found. The four trigonometric functions, produced from Eq. (32) for vector $\mathbf{b}$ of the fixed axis, are

Table 1 Five given poses

#	ϕ_j (rad)	$\mathbf{e}_j^T$	$\mathbf{r}_j^T$
1	0	[0,0,1]	[0,0,0]
2	0.2275	[−0.5516,−0.4597,0.6959]	[8.5499,4.2276,−11.3658]
3	0.3361	[−0.7508,−0.5362,0.3855]	[28.3322,12.7149,−13.0406]
4	0.3288	[−0.7629,−0.6357,−0.1169]	[41.4694,23.2247,−1.1371]
5	0.2519	[−0.4171,−0.4950,−0.7621]	[34.2001,29.1295,9.0739]

$$\begin{aligned}\Delta_1(\mathbf{b}) = {} & 0.7954\,\mathrm{c}\theta_b\mathrm{c}^2\phi_b\mathrm{s}\theta_b\mathrm{s}\phi_b + 0.2216\,\mathrm{s}^3\phi_b - 0.5388\,\mathrm{c}^3\theta_b\mathrm{c}^3\phi_b \\ & + 0.8001\,\mathrm{s}^3\theta_b\mathrm{c}^3\phi_b - 1.1618\,\mathrm{c}^2\theta_b\mathrm{c}^2\phi_b\mathrm{s}\phi_b \\ & + 0.1403\,\mathrm{c}\theta_b\mathrm{c}^3\phi_b\mathrm{s}^2\theta_b + 0.0827\,\mathrm{c}\theta_b\mathrm{c}\phi_b\mathrm{s}^2\phi_b \\ & + 0.1425\,\mathrm{s}^2\theta_b\mathrm{c}^2\phi_b\mathrm{s}\phi_b - 0.6723\,\mathrm{s}\theta_b\mathrm{c}\phi_b\mathrm{s}^2\phi_b \\ & + 0.0601\,\mathrm{c}^2\theta_b\mathrm{c}^3\phi_b\mathrm{s}\theta_b \end{aligned} \tag{39a}$$

$$\begin{aligned}\Delta_2(\mathbf{b}) = {} & 0.3726\,\mathrm{c}\theta_b\mathrm{c}^2\phi_b\mathrm{s}\theta_b\mathrm{s}\phi_b + 0.2385\,\mathrm{s}^3\phi_b - 0.6712\,\mathrm{c}^3\theta_b\mathrm{c}^3\phi_b \\ & + 0.6292\,\mathrm{s}^3\theta_b\mathrm{c}^3\phi_b - 0.5949\,\mathrm{c}^2\theta_b\mathrm{c}^2\phi_b\mathrm{s}\phi_b \\ & + 0.6866\,\mathrm{c}\theta_b\mathrm{c}^3\phi_b\mathrm{s}^2\theta_b + 0.8044\,\mathrm{c}\theta_b\mathrm{c}\phi_b\mathrm{s}^2\phi_b \\ & - 0.2671\,\mathrm{s}^2\theta_b\mathrm{c}^2\phi_b\mathrm{s}\phi_b - 1.1069\,\mathrm{s}\theta_b\mathrm{c}\phi_b\mathrm{s}^2\phi_b \\ & - 0.1149\,\mathrm{c}^2\theta_b\mathrm{c}^3\phi_b\mathrm{s}\theta_b \end{aligned} \tag{39b}$$

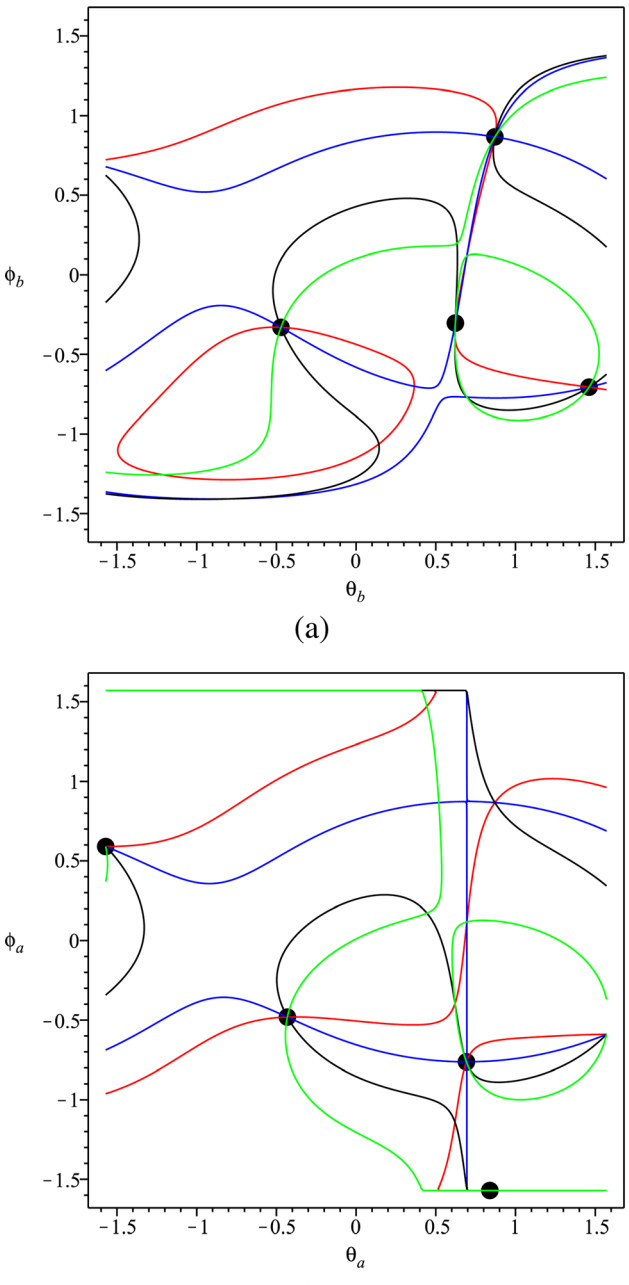

Fig. 4 Contour plots for (*a*) angles ϕ_b and θ_b, and (*b*) angles ϕ_a and θ_a

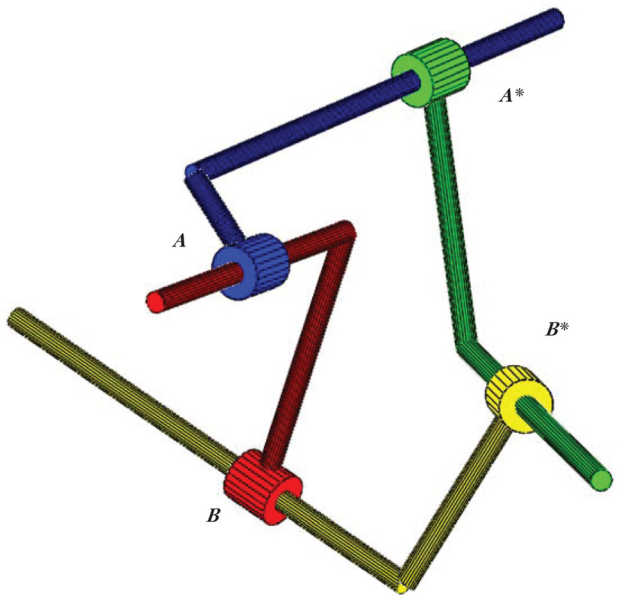

Fig. 5 A CCCC linkage for five given poses

$$\Delta_3(\mathbf{b}) = -0.1721\,c\theta_b c^2\phi_b s\theta_b s\phi_b + 0.2086\,s^3\phi_b - 0.3794\,c^3\theta_b c^3\phi_b + 0.1339\,s^3\theta_b c^3\phi_b + 0.4073\,c^2\theta_b c^2\phi_b s\phi_b + 0.8991\,c\theta_b c^3\phi_b s^2\theta_b + 0.8365\,c\theta_b c\phi_b s^2\phi_b - 0.6039\,s^2\theta_b c^2\phi_b s\phi_b - 0.9426\,s\theta_b c\phi_b s^2\phi_b - 0.2169\,c^2\theta_b c^3\phi_b s\theta_b \quad (39c)$$

$$\Delta_4(\mathbf{b}) = -0.4783\,c\theta_b c^2\phi_b s\theta_b s\phi_b + 0.1969\,s^3\phi_b - 0.0680\,c^3\theta_b c^3\phi_b - 0.1912\,s^3\theta_b c^3\phi_b + 0.6195\,c^2\theta_b c^2\phi_b s\phi_b + 0.5308\,c\theta_b c^3\phi_b s^2\theta_b + 0.4241\,c\theta_b c\phi_b s^2\phi_b - 0.5335\,s^2\theta_b c^2\phi_b s\phi_b - 0.3676\,s\theta_b c\phi_b s^2\phi_b - 0.2046\,c^2\theta_b c^3\phi_b s\theta_b \quad (39d)$$

The foregoing equations involve sixth-order expressions of the harmonic functions of θ_b and φ_b. In this light, if the tan-half identities [29] are introduced, Eqs. (39*a*)–(39*d*) become bivariate polynomial equations of the 12th degree. This means that the Bezout number of any pair of these is $12^2 = 144$, the resolvent polynomial of the two thus being monovariate, but of 144th degree. It is well known [40] that polynomial-root finding is inherently ill-conditioned, i.e., extremely sensitive to round-off error in the coefficients, as the polynomial degree becomes moderately large, of 10 or higher. The semigraphical method proposed here comes to the rescue. The four contours stemming from Eqs. (39*a*)–(39*d*) are shown in Fig. 4(*a*). Four intersections can be identified, which suggests four real solutions, for which accurate values are found with a nonlinear least-square solver—as per the discussion in Sec. 4.1 in connection with the solution of Eq. (30)—namely, Maple's "LSSolve." The contour plots for vector $\mathbf{a}_0$ are shown in Fig. 4(*b*). Identifying the intersection around $\varphi_a = \pm\pi/2$, where all four contours are superimposed along the line $\varphi_a = \pm\pi/2$, requires special attention. While there are infinitely many intersections, all correspond to one unique solution, $\mathbf{a}_0 = [0,0,-1]^T$, no matter what value θ_a takes. This is the special case discussed in Sec. 4.1, which shows that the semigraphical method is able to cope with special cases.

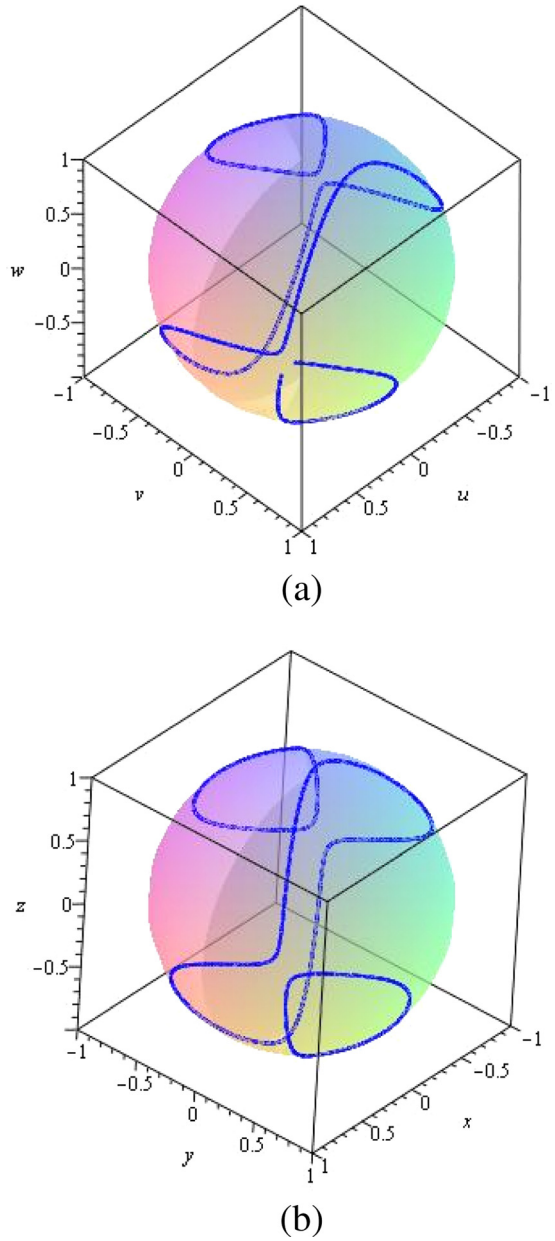

Fig. 6 Centerpoint and circlepoint spherical curves

A total of four real solutions are found for the unit vectors of the mobile and fixed-joint axes. These solutions are matched through Eq. (8a) into four sets, each being a CC-dyad solution. From these solutions, the moment components of the two axes of the CC dyad are found from Eq. (14), with

Table 2 CCCC linkage solutions

#	$\mathbf{a}_0$	$\mathbf{b}$	$\bar{\mathbf{a}}_0$	$\bar{\mathbf{b}}$
1	[0.557,0.461,−0.691]	[0.775,0.557,−0.299]	[−16.724,5.525,−9.784]	[−24.798,1.756,−61.078]
2	[0.805,−0.370,−0.463]	[0.843,−0.430,−0.324]	[−27.809,39.395,−79.918]	[−22.408,35.386,−105.146]
3	[0.000,0.000,−1.000]	[0.417,0.495,0.762]	[0.000,0.000,0.000]	[−24.109,−19.553,25.894]
4	[0.000,−0.831,0.557]	[0.083,0.756,−0.649]	[−24.925,29.496,44.034]	[19.108,−22.451,−23.685]

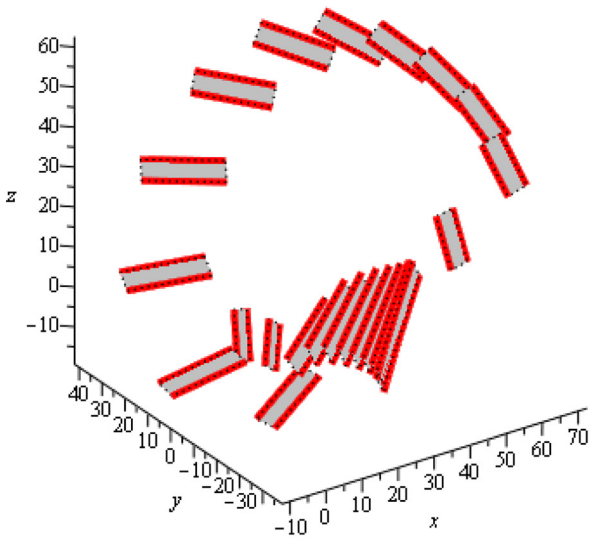

(a)

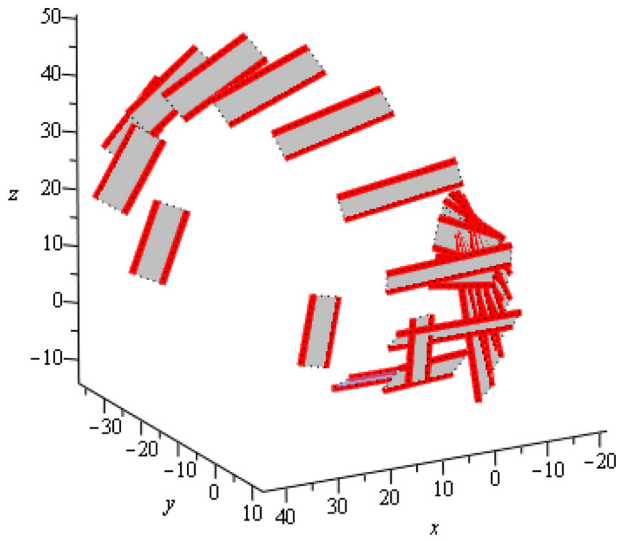

(b)

Fig. 7 Congruences of (*a*) the fixed axis; and (*b*) the moving axis

$$\mathbf{M} = \begin{bmatrix} 0.0491 & -0.0883 & -0.0194 & -0.0009 & 0.0013 & 0.0001 \\ 0.0164 & -0.0258 & -0.0041 & 0.0715 & -0.0981 & 0.0027 \\ -0.0867 & 0.1041 & -0.0003 & 0.1555 & -0.1943 & 0.0416 \\ -0.1622 & 0.1666 & -0.0194 & 0.1545 & -0.1932 & 0.0409 \\ 0.5566 & 0.4613 & -0.6909 & 0 & 0 & 0 \\ 0 & 0 & 0 & 0.7752 & 0.5565 & -0.2987 \end{bmatrix} \tag{40}$$

$$\mathbf{w} = [-1.1049, -2.4925, -4.7123, -2.8470, 0, 0]^T \tag{41}$$

Equation (41) displays matrix $\mathbf{M}$ and vector $\mathbf{w}$ produced from the direction solution #1. The corresponding moments can be directly obtained from $\mathbf{x} = \mathbf{M}^{-1}\mathbf{w}$. All dual vectors of the moving and fixed axes are listed in Table 2. A total of six CCCC mechanisms can be synthesized from the four sets of solutions. A mechanism generated from solutions #3 and #4 is shown in Fig. 5. Note that this example takes advantage of the RCCC linkage reported in Ref. [26]. The mechanism shown in Fig. 5, identical to a linkage in Ref. [26], validates the method developed in this work.

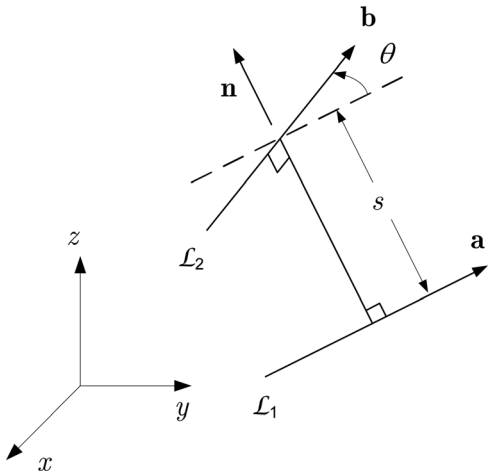

Fig. 8 The dual angle between two lines

5.2 Four-Pose Case. The synthesis of CCCC linkages with four poses was conducted using as data the first four rows of Table 1. For the four given poses, the associated centerpoint- and circlepoint curves are displayed in Fig. 6, on the unit sphere. Of these, the circlepoint curve is selected to generate the congruences of lines. Figure 7 shows the congruences of the fixed and moving axes, where solid edges of each plane indicate the direction of the set of lines. Note that 24 points are selected from the centerpoint curve to generate the congruences.

6 Discussion and Conclusions

The spatial Burmester problem was formulated using dual algebra, then *robustly* solved using a semigraphical approach. The synthesis equations were derived for different types of spatial dyads, CC, CR, and RR. A synthesis method of spatial linkages applicable to CCCC and RCCC linkages was developed. The method consists of two steps: direction-equation solving and moment-equation solving. An example included in the paper shows that the method is able to cope with the special cases involving none or infinitely many solutions.

A contribution of the paper lies in the formulation of the synthesis equations, from which the congruences of lines to determine fixed and moving axes can be generated. The formulation, expressed in terms of direction and moments of axes of rotation, reveals the geometric relationship between the synthesis tasks and the possible solutions. It was shown that the semigraphical approach, employed in equation-solving, provides a robust means of obtaining all possible solutions, including the case of CCCC linkages with four given poses.

While the overall approach emphasizes robustness, there is an element of arbitrariness that hampers the concept: the x-component of $\bar{\mathbf{a}}_0$ was arbitrarily set to λ when finding the congruences, but any other component of this moment, or of $\bar{\mathbf{b}}$ for that matter, could have been chosen. This shortcoming can be fixed, but we have not elaborated on it for the sake of conciseness.

Finally, notice that: (i) the CC dyad can meet up to five given poses; (ii) the RC dyad can meet up to three given poses; and (iii) the spatial counterpart of the planar, or spherical for that matter, four-bar linkage is the RCCC linkage. In this light, then, the RCCC linkage can visit up to three given poses of its coupler link.

Appendix A: A Summary of Dual Algebra

Some fundamental concepts of dual algebra are summarized here. More details can be found in Refs. [4,35,36].

A dual number $\hat{a}$ is defined as the sum of a primal part a, and a dual part $\bar{a}$, namely

$$\hat{a} = a + \varepsilon \bar{a} \tag{A1}$$

where ε is the dual unity, which verifies $\varepsilon \neq 0$ and $\varepsilon^2 = 0$, while a and $\bar{a}$ are real numbers, the former being the primal part of $\hat{a}$, the latter its dual part.

The dual angle $\hat{\theta}$ between two skew lines $\mathcal{L}_1$ and $\mathcal{L}_2$ is defined as

$$\hat{\theta} = \theta + \varepsilon s \tag{A2}$$

where θ and s are, respectively, the twist angle and the distance between the two lines, as shown in Fig. 8.

A dual function of a dual argument, $\hat{f}(\hat{x})$, is defined as

$$\hat{f}(\hat{x}) = f(x) + \varepsilon f'(\bar{x}) \tag{A3}$$

In this vein, the dual trigonometric functions of the dual angle $\hat{\theta}$ become

$$\cos\hat{\theta} = \cos\theta - \varepsilon s \sin\theta; \quad \sin\hat{\theta} = \sin\theta + \varepsilon s \cos\theta \tag{A4}$$

Moreover, all identities for ordinary trigonometry hold for dual angles.

A dual vector $\hat{\mathbf{a}}$ is defined as the sum of a primal vector part $\mathbf{a}$, and a dual-vector part $\bar{\mathbf{a}}$, namely

$$\hat{\mathbf{a}} = \mathbf{a} + \varepsilon \bar{\mathbf{a}} \tag{A5}$$

where both $\mathbf{a}$ and $\bar{\mathbf{a}}$ are Cartesian, three-dimensional real-valued vectors.

Dual vectors can be used to represent a line. The six normalized Plücker coordinates [4] of a line $\mathcal{L}$ passing through a point P of position vector $\mathbf{p}$ and parallel to the unit vector $\mathbf{e}$ are given by the pair $(\mathbf{e}, \mathbf{p} \times \mathbf{e})$, where the product $\bar{\mathbf{e}} = \mathbf{p} \times \mathbf{e}$ denotes the moment of the line with respect to the origin. The foregoing coordinates can be represented by a dual unit vector $\hat{\mathbf{e}}$, whose six real components are the Plücker coordinates of $\mathcal{L}$, namely

$$\hat{\mathbf{e}} = \mathbf{e} + \varepsilon \mathbf{e}, \quad \text{with} \quad \|\mathbf{e}\| = 1, \quad \mathbf{e}^T \bar{\mathbf{e}} = 0 \tag{A6}$$

For two lines $\mathcal{L}_1$ and $\mathcal{L}_2$, let $\hat{\mathbf{a}}$ and $\hat{\mathbf{b}}$ be their dual-vector representation, as depicted in Fig. 8. The relations below hold

$$\hat{\mathbf{a}}^T \hat{\mathbf{b}} = \cos\hat{\theta}, \quad \hat{\mathbf{a}} \times \hat{\mathbf{b}} = \hat{\mathbf{n}} \sin\hat{\theta} \tag{A7}$$

where $\hat{\theta}$ is the dual angle between lines $\mathcal{L}_1$ and $\mathcal{L}_2$, while $\hat{\mathbf{n}}$ is the dual unit vector of the common normal to the two lines, which is given by

$$\hat{\mathbf{n}} = \frac{1}{\sin\hat{\theta}} (\hat{\mathbf{a}} \times \hat{\mathbf{b}}) \tag{A8}$$

That is

$$\hat{\mathbf{n}} = \frac{1}{\sin\theta + \varepsilon s \cos\theta} (\mathbf{a} + \varepsilon \hat{\mathbf{a}}) \times (\mathbf{b} + \varepsilon \bar{\mathbf{b}}) \tag{A9}$$

Expanding the right-hand side of the above equation yields, after simplification

$$\hat{\mathbf{n}} = \frac{1}{\sin\theta} (\mathbf{a} \times \mathbf{b}) + \varepsilon \left(\frac{1}{\sin\theta} (\mathbf{a} \times \bar{\mathbf{b}} + \bar{\mathbf{a}} \times \mathbf{b}) - \frac{s\cos\theta}{\sin^2\theta} (\mathbf{a} \times \mathbf{b}) \right) \tag{A10}$$

or, in compact form

$$\hat{\mathbf{n}} = \mathbf{n} + \varepsilon \bar{\mathbf{n}} \tag{A11}$$

with

$$\mathbf{n} = \frac{1}{\sin\theta} (\mathbf{a} \times \mathbf{b}), \quad \bar{\mathbf{n}} = \frac{1}{\sin\theta} (\mathbf{a} \times \bar{\mathbf{b}} + \bar{\mathbf{a}} \times \mathbf{b}) - \frac{s\cos\theta}{\sin^2\theta} (\mathbf{a} \times \mathbf{b}) \tag{A12}$$

Appendix B: Synthesis Equation of RR Dyads

The additional constraint equations for RR dyads can be derived from the zero-sliding condition, using the same approach as in the case of RC dyads discussed in Sec. 3.2. Alternatively, the constraint equations can be derived from the geometric relationship between two axes. With reference to Fig. 3, where B and N are intersections of the common normal with lines $\mathcal{L}_a$ and $\mathcal{L}_b$, if point A_0 is coincident with N at the reference configuration, these two points will remain coincident for all poses. As line NB is the common normal to the two axes, the constraints are expressed as

$$\mathbf{a}_j^T (\mathbf{r}_{Aj} - \mathbf{r}_B) = 0, \quad \mathbf{b}^T (\mathbf{r}_{Aj} - \mathbf{r}_B) = 0, \quad j = 0, \ldots, m \tag{B1}$$

where $\mathbf{r}_{Aj} = \mathbf{r}_j + \mathbf{Q}_j \mathbf{r}_{A0}$. Equations (B1), together with Eqs. (8*a*) and (11), build up the system of synthesis equations for RR dyads.

References

[1] McCarthy, J. M., 2011, "21st Century Kinematics: Synthesis, Compliance, and Tensegrity," ASME J. Mech. Rob., **3**(2), 020201.

[2] Pisla, D., Ceccarelli, M., Husty, M., and Corves, B., 2010, "New Trends in Mechanism Science: Analysis and Design," *Mechanisms and Machine Science*, Springer, New York.

[3] Kocabas, H., 2009, "Gripper Design With Spherical Parallelogram Mechanism," ASME J. Mech. Des., **131**(7), 075001.

[4] McCarthy, J. M., and Soh, G. S., 2011, *Geometric Design of Linkages*, Springer, New York.

[5] Angeles, J., 1982, *Spatial Kinematic Chains: Analysis, Synthesis, and Optimisation*, Springer-Verlag, Berlin.

[6] Suh, C. H., and Radcliffe, C. W., 1978, *Kinematics and Mechanisms Design*, Wiley, New York.

[7] Bottema, O., and Roth, B., 1979, *Theoretical Kinematics*, North-Holland, New York.

[8] Hunt, K. H., 1978, *Kinematic Geometry of Mechanisms*, Oxford University Press, New York.

[9] Lichtenheldt, W., 1967, *Konstruktionslehre der Getriebe*, Akademie-Verlag, Berlin.

[10] Sandor, G. N., and Erdman, A. G., 1984, *Advanced Mechanism Design: Analysis and Synthesis*, Vol. 2, Prentice-Hall, New Jersey.

[11] Ravani, B., and Roth, B., 1983, "Motion Synthesis Using Kinematic Mappings," ASME J. Mech., Transm., Autom. Des., **105**, pp. 460–467.

[12] Hayes, M. J. D., and Zsombor-Murray, P. J., 2002, "Solving the Burmester Problem Using Kinematic Mapping," Proceedings of DETC'2002, Montreal, Paper No. MECH-34378.

[13] Huang, C., and Huang, B., 2009, Spatial Generalization of the Planar Path Generation Problem, *Computational Kinematics*, A. Kecskeméthy, and A. Muller, ed., Springer, New York, pp. 117–124.

[14] Myszka, D. H., Murray, A. P., and Schmiedeler, J. P., 2009, "Assessing Position Order in Rigid Body Guidance: An Intuitive Approach to Fixed Pivot Selection," J. Mech. Des., **131**(1), 014502.

[15] Chen, C., Bai, S., and Angeles, J., 2008, "A Comprehensive Solution of the Classic Burmester Problem," CSME Trans., **32**(2), pp. 137–154.

[16] Hartenberg, R. S., and Denavit, J., 1964, 1967, " Kinematic Synthesis of Linkages, McGraw-Hill, New York.

[17] Zimmerman, J. R., 1967, "Four-Precision-Point Synthesis of the Spherical Four-Bar Function Generator," J. Mech., **2**(1), pp. 133–139.

[18] Chiang, C. H., 1988, Kinematics of Spherical Mechanism, Cambridge University Press, Cambridge.

[19] Meyer zur Capellen, W., and Dittrich, G., 1970, "Adjustable Spherical Four-Bar Linkage," *Bulletin of Mechanical Engineering Education*, Pergamon Press, Oxford, pp. 341–342.

[20] Angeles, J., and Bai, S., 2010, "A Robust Solution of the Spherical Burmester Problem," Proceedings of ASME DETC2010, Montreal, Paper No. MECH-28189.

[21] Brunnthaler, K., Schrocker, H. P., and Husty, M., 2006, "Synthesis of Spherical Four-Bar Mechanisms Using Spherical Kinematic Mapping," *Advances in Robot Kinematics*, J. Lennarcic and B. Roth, ed., Springer, The Netherlands, pp. 377–384.

[22] Tipparthi, H., and Larochelle, P., 2011, "Orientation Order Analysis of Spherical Four-Bar Mechanisms," ASME J. Mech. Rob., **3**(4), 044501.

[23] Perez, A., and McCarthy, J. M., 2003, "Dimensional Synthesis of Bennett Linkages," ASME J. Mech. Des., **125**(1), pp. 98–104.

[24] Brunnthaler, K., Schrocker, H. P., and Husty, M., 2005, "A New Method for the Synthesis of Bennett Mechanisms," Proceedings of CK2005 International Workshop on Computational Kinematics, Cassino, Italy.

[25] Tsai, L. W., and Roth, B., 1972, "Design of Dyads With Helical, Cylindrical, Spherical, Revolute and Prismatic Joints," Mech. Mach. Theory, **7**(1), pp. 85–102.
[26] Jamalov, R. I., Litvin, F. L., and Roth, B., 1984, "Analysis and Design of RCCC Linkages," Mech. Mach. Theory, **19**(4-5), pp. 397–407.
[27] Innocenti, C., 1995, "Polynomial Solution of the Spatial Burmester Problem," ASME J. Mech. Des., **117**(1), pp. 64–68.
[28] Larochelle, P. M., 1995, "On the Design of Spatial 4C Mechanisms for Rigid-Body Guidance Through 4 Positions," *Proceedings of 1995 ASME Design Engineering Technical Conferences*, Boston, MA, pp. 825–832.
[29] Wampler, C. W., Morgan, A. P., and Sommese, A. J., 1990, "Numerical Continuation Methods for Solving Polynomial Systems Arising in Kinematics," ASME J. Mech. Des., **112**(1), pp. 59–68.
[30] Murray, A.P., and McCarthy, J. M., 1994, "Five Position Synthesis of Spatial CC Dyads," *Proceedings of ASME Mechanisms Conference*, Minneapolis, MN, pp. 143–152.
[31] Roth, B., 1967, "Finite Position Theory Applied to Mechanism Synthesis," ASME J. Appl. Mech., 34(3), pp. 599–605.
[32] Roth, B., 1967, "The Kinematics of Motion Through Finitely Separated Positions," ASME J. Appl. Mech., **34**(3), pp. 591–598.
[33] Pottmann, H., and Wallner, J., 2001, *Computational Line Geometry*, Springer-Verlag, Heidelberg, Berlin.
[34] Tsai, L. W., and Roth, B., 1973, "Incompletely Specified Displacements: Geometry and Spatial Linkage Synthesis," ASME J. Eng. Ind., **95**(B), pp. 603–611.
[35] Angeles, J., 1998, "The Application of Dual Algebra to Kinematic Analysis," *Computational Methods in Mechanical Systems*, J. Angeles and E., Zakhariev, ed. Springer-Verlag, Heidelberg, pp. 3–31.
[36] Fischer, I. S., 1999, *Dual-number Methods in Kinematics, Statics, and Dynamics*, CRC Press, Boca Raton, FL.
[37] Pennestrì, E., and Stefanelli, R., 2007, "Linear Algebra and Numerical Algorithms Using Dual Numbers," Multibody Syst. Dyn., 18, pp. 323–344.
[38] Nash, S. G., and Sofer, A., 1996, *Linear and Nonlinear Programming*, McGraw-Hill, New York.
[39] Angeles, J., 2002, *Fundamentals of Robotic Mechanical Systems*, Springer-Verlag, New York.
[40] Forsythe, G. E., 1970, "Pitfalls in Computation, or Why a Math Book Isn't Enough," Am. Math. Monthly, **27**, pp. 931–956.